Geochimica et Cosmochimica Acta Vol. 53, pp. 3115–3130

0016-7037/89/$3.00 + .00

Determination of trace element mineral/liquid partition coefficients in melilite and diopside by ion and electron microprobe techniques

S. M. KUEHNER,[1] J. R. LAUGHLIN,[2] L. GROSSMAN,[1] M. L. JOHNSON,[3] and D. S. BURNETT[3]

[1]Department of the Geophysical Sciences, University of Chicago, Chicago, IL 60637, U.S.A.
[2]Department of Chemistry, University of Chicago, Chicago, IL 60637, U.S.A.
[3]Department of Geological and Planetary Sciences, California Institute of Technology, Pasadena, CA 91125, U.S.A.

(*Received February* 6, 1989; *accepted in revised form September* 15, 1989)

Abstract—The use of the ion microprobe for quantitative analysis of Sr, Y, Zr, La, Sm, and Yb in melilite and pyroxene is evaluated. Three trace element-doped synthetic glasses of composition Ak_{40}, Ak_{80}, and Di_2AbAn were analyzed by ion microprobe (IMP) using ion yields determined from Corning glass standards. IMP-determined oxide concentrations in the Di_2AbAn glass agree well with electron microprobe (EMP) analyses (to within 6%), but IMP analyses of the melilite glasses deviate from EMP averages by up to 19%. The deviations are due to erroneous SiO_2 estimates caused by suppression of Si ion intensities by the enhanced concentrations of Ca and Al in the melilite glasses compared to the standards. Thus, in order to determine compositions of melilite, diopside, and glass from subliquidus experiments on each of the three starting compositions, we adopted a new set of ion yields such that IMP analyses of the three starting glasses reproduce the EMP average compositions. Further IMP and EMP comparisons of the subliquidus assemblages show that quantitative analyses of melilite, diopside, and glass can be obtained by IMP that are within 10% of the concentrations obtained by EMP, when ion yields determined from glass starting compositions are used. EMP-IMP comparison of crystal and glass analyses also suggests that a structural matrix effect may result in overestimation of SrO (10–12%) in melilite by IMP.

Comparison of our data for Ak_{12} and Ak_{90} melilite compositions with literature results shows that melilite/liquid D-values for REE^{3+} determined by IMP decrease with increasing X_{Ak} (Ak_{90}: $D_{La} = 0.038$, $D_{Sm} = 0.032$, $D_{Yb} = 0.0086$; Ak_{12}: 0.67, 0.75, 0.25, respectively) while that for Sr (=Eu^{2+}) changes only slightly (0.99 to 0.78, respectively). Since X_{Ak} increases with decreasing temperature for all melilite with $X_{Ak} < 0.7$, a progressively larger positive Eu anomaly is predicted for melilite as it crystallizes with falling temperature. Our diopside/liquid data are characterized by a large degree of scatter on most interelement correlation plots of apparent partition coefficients. The data cannot be understood in terms of simple models of boundary layer formation but require a complex surface partitioning explanation. Nevertheless, estimates of diopside/liquid D-values are in excellent agreement with literature data.

INTRODUCTION

EQUILIBRIUM PARTITIONING of trace elements between crystals and coexisting liquids has been used extensively to model the chemical evolution of a magma brought about by crystal fractionation processes. In favorable circumstances, differences in whole-rock trace element concentrations between samples from a given magmatic center can be assessed in terms of fractionation of liquidus phase assemblages. Results of these studies may indicate, for example, a history of high pressure crystal fractionation of phases for which there may be no petrographic evidence (SHERATON et al., 1984), or provide evidence for complex partial melting and magma chamber processes (LANGMUIR et al., 1977; PANKHURST, 1977).

Experimental studies by STOLPER (1982) and STOLPER and PAQUE (1986) show that some Ca-, Al-rich inclusions (CAIs) in carbonaceous chondrites represent closed-system, essentially total-crystallization products of partially molten droplets. With such presumably simple magmatic systems, studying the trace element evolution of the liquid during CAI solidification should permit a sophisticated level of understanding of the igneous processes. Alternatively, Type B CAIs originating by processes other than igneous crystallization may also be identifiable. Unlike terrestrial differentiation studies, however, separate aliquots of bulk material produced during successive stages of crystallization inside single Type B inclusions are not available for analysis. The progressive change in liquid composition must instead be inferred by examining trace element zoning profiles within the crystallizing phases of the inclusion. In this case, it is necessary not only to understand quantitatively how trace elements are partitioned between crystals and liquid, as in terrestrial studies, but it is also necessary to be able to obtain accurate analyses of trace elements at ppm concentrations from 'spot' locations in single crystals. The purpose of this paper is to evaluate the use of the ion microprobe in obtaining quantitative analyses of trace elements from the dominant phases in Type B CAIs, melilite and clinopyroxene. We also have utilized our results to investigate the partitioning behavior of selected elements between these phases and coexisting liquid.

Application of the ion microprobe to quantitative analysis of major and trace elements in geological samples has been evaluated in several studies, e.g. SHIMIZU et al. (1978), STEELE et al. (1981), RAY et al. (1983), and ZINNER and CROZAZ (1986). Routine quantitative chemical analyses by ion microprobe have been hindered by the poorly defined roles of structural and chemical matrix effects on ion yields and by molecular ion interferences with analytical peaks of elemental ions. To evaluate these factors for eventual analysis of melilite and clinopyroxene in natural Type B inclusions, we have

undertaken a combined electron probe-ion probe study of these phases produced from synthetic CMAS and NaCMAS liquids doped with Sr, Zr, Y, La, Sm, and Yb at 0.30–1.3 oxide wt% levels. At these concentrations, crystals and glass can be characterized initially by electron microprobe analysis (EMP). Subsequent ion microprobe analyses (IMP) of the synthetic products can then be compared to results obtained by EMP and variables affecting the ion probe determinations adjusted, if necessary, to reproduce the compositions obtained by electron probe. In principle, identical spots can be analyzed by both techniques, eliminating possible problems associated with sample heterogeneity. The synthetic melilite and clinopyroxene samples can then be used as standards for ion probe analyses of the same phases in natural CAIs in which concentrations of these elements are too low for accurate analysis by the electron microprobe. Preliminary results of this study were reported by KUEHNER et al. (1988).

EXPERIMENTAL

Synthesis

Synthetic melilite crystals were grown from two starting compositions, Ak_{40} and Ak_{80} (molar), and diopside was grown from a Di_2AbAn (molar) composition. Minor elements were added to synthetic oxide mixes of each starting composition by means of a nitric acid solution and the mixtures dried in open Pt tubes at 1000°C. To ensure chemical homogeneity in the starting mixes, the dried powders were fused in sealed Pt tubes at 1310°C and finely ground in a ball mill. The fusion and grinding process was then repeated. Experiments were performed in a 1 atm furnace. In order to reduce the number of crystal nuclei in the charge and provide for growth of fewer but larger crystals more suited for IMP analysis, the general synthesis procedure (see footnotes to Table 4 for details) was first to hold the sample at a temperature slightly above the liquidus for 1–2 h. The temperature was then reduced such that the charge rapidly entered the melilite + liquid or diopside + liquid phase field. Following a 5–28 h period, the charge was quenched. This type of thermal history is not optimum for partition coefficient studies due to the possibility of boundary layer development during rapid crystal growth when the charge enters the temperature regime of the two-phase field. Nevertheless, samples suitable for electron probe/ion probe comparison were produced. In a synthesis more suitable for partition coefficient measurements (JONES and BURNETT, 1987), the temperature in one diopside synthesis experiment, 35-5B, was dropped about 10 C° from a slightly superliquidus temperature in order to produce seed crystals, then reduced slowly to a temperature 65°C below the liquidus.

Electron microprobe methods

Because the quality of the ion probe analyses of the synthetic run products depends on the quality of electron probe analyses, considerable care was taken in the setup procedures of the latter instrument. All samples and standards were analyzed using wavelength dispersive techniques on an automated CAMECA SX-50 electron microprobe at the University of Chicago. Operating conditions were 15 kV, 25 nA and 30 sec peak and background counting times for major elements (Na, Mg, Al, Si, Ca) and 25 kV, 200 nA and 120–360 sec for minor elements (Table 1). The beam diameter was fixed at 5 μm for each routine. Step-scans of count rates were collected up to 1200 sin θ units on either side of the peak position and background offsets were placed symmetrically about the peak at positions free of interfering spectral lines. It was not possible to locate Sr $L\alpha_1$ background positions by this method due to interference with a Si K_β satellite peak on the low sin θ side of the Sr peak. Background counts for Sr $L\alpha_1$ were obtained by collecting counts at the high sin θ position and assuming a flat background under the peak. The soundness of this approach was verified by analysis of Sr-free standards.

Amelia albite and synthetic glass standards were used in calibration of the analyzed elements (Table 1). With the exception of Na, a calibration was not accepted until analysis of the standard, as an unknown, reproduced the calibration count rate to within 1%. Because of the mobility of Na under electron bombardment, up to a 2% difference in count rates was accepted for this element. Sodium migration under the electron beam was not specifically evaluated, but was minimized by putting Na first in the analysis routine and by using a 5 μm wide beam. Oxide totals from Na-bearing samples and standards rule out large amounts of Na loss under these analytical conditions. The possibility of minor element mobility under the 25 kV, 200 nA conditions was only examined through replicate analysis of several spots. No consistent or significant variation in minor element concentrations was observed.

Superliquidus quench glasses of each starting composition were analyzed in two stages with the electron microprobe. Each sample was first analyzed for major elements, and the coordinates of each point recorded. Operating conditions were then adjusted for minor element analyses and the previously stored points relocated. All other samples were analyzed using an automatic two-condition analysis routine in which major elements were determined, the current and accelerating voltage were changed, and minor elements were determined before moving to the next spot. Each analytical routine automatically checks, and updates if necessary, the beam current to the desired run conditions at the onset of each analysis. Beam currents

TABLE 1 Operating Conditions for the Electron Microprobe

	Standard*	Standard Conc. (wt %)	Crystal	Counting Time (sec)	Background Offsets#	Minimum Detection Limit## (wt %)	Unc.† (2σ)
Na_2O	Amelia Albite	11.67	TAP	30	600	---	0.02
MgO	Diopside Glass	18.62	TAP	30	1000	---	0.09
Al_2O_3	Amelia Albite	19.42	TAP	30	1000	---	0.15
SiO_2	Amelia Albite	68.71	TAP/PET	30	900	---	0.15
CaO	Diopside Glass	25.90	PET	30	500	---	0.24
SrO	X-Glass	0.804	PET	120	400**	0.004	0.010
Y_2O_3	REE 3	4.076	PET	120	400	0.006	0.010
ZrO_2	X-Glass	0.784	PET	120	500	0.004	0.018
La_2O_3	REE 3	4.280	LIF	180	800	0.006	0.013
Sm_2O_3	REE 2	4.256	LIF	180	450	0.008	0.008
Yb_2O_3	REE 2	4.259	LIF	360	550	0.001	0.004

* Amelia Albite -- natural; ref: Smith and Ribbe (1966).
Diopside Glass -- synthetic; prepared by J. Boyd, Geophysical Lab.
X-Glass -- synthetic; made by Corning Glass and distributed by A. Chodos at Cal Tech.
REE 2, REE 3 -- synthetic glasses; ref: Drake and Weill (1972).

** Background counted only on 1 side of peak, peak counts determined by assuming a flat background.

10^5 Sinθ

Calculated following Reed (1973); values apply to all analyzed samples.

† Typical analytical uncertainty for melilite and diopside samples based on counting statistics for a single analysis.

during a time period equivalent to one analysis (18 min) were found to be within 1% of the nominal value.

Ion probe methods

Ion probe analyses were obtained with a modified AEI IM-20 instrument at the University of Chicago, using a mass filtered $^{16}O^-$ primary beam and an accelerating voltage of 20 kV (HINTON et al., 1988). A sample current of 20 nA, which produced an elliptical beam spot of $\sim 20 \times 30$ μm, was used in analyses of the quenched starting glasses. Because of the increased spatial resolution required for crystal/glass samples, the primary beam current was reduced to 10 nA for these analyses, making a spot size of 10×15 μm. All samples and standards were carbon coated.

A critical condition for quantitative ion probe analyses at low mass resolution (300–500) is the elimination of molecular ion interferences at the nominal masses of elemental ions. Secondary molecular ions produced from silicate matrices possess, in general, less kinetic energy than monatomic ions (SHIMIZU et al., 1978) and, consequently, molecular interferences can in most cases be suppressed by making measurements at high ion energies. Instrument settings for this study, in which the composition of the samples was known (Table 2), were determined by first making a preliminary computer controlled mass scan from mass 200 through mass 7 on glass sample 35-1, counting at each mass for one second. This scan identified all elements in the sample, as well as many molecular interferences. A second mass scan was then obtained using energy filtering. This resulted in the suppression of molecular ion intensities by factors of 275–1000, while the intensity of monatomic ions was reduced only by factors of 20–100. On the Chicago instrument, energy filtering is produced by adjusting the voltage across a small wire located close to the beam spot. The absolute energy of transmitted ions cannot be determined by this device, but HINTON et al. (1988) estimate that it is $\sim$30 eV. The efficiency of energy filtering in eliminating molecular interferences was evaluated by comparing the ratio of count rates of different isotopes of a particular element to the known ratio of their isotopic abundances. Of 28 isotopic ratios measured with energy filtering for 7 elements, 22 ratios were within 10% of their expected values. Of the latter, 20 ratios were within 2σ counting uncertainties of their expected values. Each of the six isotopes whose ratios differed by more than 10% was of low abundance, accounting for no more than 6% of the total natural abundance of the element. These isotopes were not used for quantitative analyses. This comparison shows that the analytical technique used in this study was successful in reducing molecular interferences to acceptable levels. Thus, using the most intense peaks for analysis, any contribution from molecular interferences is insignificant. The mono-isotopic elements Na, Al, and Y were assumed to be interference-free.

During quantitative analyses, intensities were measured at the following masses: ^{174,172}Yb, ^{154,152}Sm, ^{139}La, ^{94,92,91,90}Zr, ^{89}Y, ^{88,87,86}Sr, ^{40}Ca, ^{30,28}Si, ^{27}Al, ^{25,24}Mg, ^{23}Na. Each scan cycled from mass 200 to mass 7 with two-second counts at each of the nominal mass positions of interest. Each analysis is the result of summing the counts collected from 5–10 scans through the mass spectrum. Background and deadtime were negligible. Uncertainties in IMP data due to counting statistics are <2%, except for Zr in melilite where they reach a maximum of 5%.

Absolute intensities of an element in a given matrix can be highly variable, on a day-to-day basis, due to subtle differences in instrument tuning. Therefore, the intensities of secondary ions are typically normalized to a single element. As the number of Ca cations in the structural formula of melilite is constant throughout the gehlenite-akermanite solid solution series (2.000), we assumed the Ca concentration in melilite analyses and normalized our intensity data to ^{40}Ca. For glass analyses, intensity data were normalized to ^{40}Ca but no assumption of Ca content was made. All analyses were re-normalized to 100%. Relative ion yields for Ca, Al, Mg, Si, and La used in analysis of the quenched starting glasses (Table 3) were determined from Corning V-, W-, and X-glasses. Ion yields used in analysis of Sm and Yb were estimated from the ion yield of La (HINTON et al., 1988); the ion yield of Na was extrapolated from the values of Rb and K as determined from the Corning X- and V-glasses, respectively. Although adjustments to the values of the ion yields were subsequently made for analyses of crystal-bearing samples, the Corning glass standards were analyzed at the beginning of each day to check for consistency in instrument tuning: relative ion yields obtained from the standard glasses changed by <5% on a day-to-day basis.

RESULTS

Glasses

The range and mean concentration of each element oxide in the superliquidus glasses made from each starting mix as

TABLE 2 Starting Compositions Determined by Electron Microprobe Analyses of Synthetic Glasses*

	*35-1**		*Ak_{40}-1***		*Ak_{80}-1****	
	Avg	Range (2σ) †	Avg	Range (2σ)	Avg	Range (2σ)
SiO_2	52 4	(51.5-54.6) (8)	28 8	(28.1-29 6) (.8)	39 0	(38.3-39 5) (6)
Al_2O_3	13 52	(13.31-14.30) (19)	21 03	(20.79-21 20) (.21)	7 11	(7.00-7 21) (10)
MgO	8.87	(8.73-9.56) (.13)	5 79	(5.65-5 90) (12)	11 31	(11 17-11 44) (11)
CaO	17.93	(17.72-18.14) (.19)	39 45	(38.78-39.83) (49)	39.24	(39 06-39 38) (19)
Na_2O	3.04	(2.22-3.29) (.33)	—		—	
SrO	701	(684-.712) (014)	674	(.646-.689) (018)	599	(577- 620) (.018)
Y_2O_3	.334	(.305-.361) (.026)	341	(.319-.363) (.020)	271	(250-.284) (016)
ZrO_2	1 33	(1.21-1.46) (13)	1 32	(1.27-1 35) (.04)	1 01	(.960-1 04) (04)
La_2O_3	.958	(.932- 984) (.024)	945	(928- 964) (.018)	.770	(756-.789) (014)
Sm_2O_3	944	(921- 968) (022)	924	(909-.939) (014)	741	(.727- 755) (.012)
Yb_2O_3	915	(.897- 936) (022)	.880	(.870- 892) (010)	697	(.690- 704) (.008)
TOT	100 94		100.15		100.75	
N	35		45		30	

Run Conditions
*35-1 1.3 hr @ 1318 °C, air quench **Ak_{40}-1 1 hr @ 1526 °C, water quench. ***Ak_{80}-1: 1 25 hr @ 1417 °C, water quench
† Two standard deviations of an individual analysis.

TABLE 3 Comparison of secondary ion yields (relative to Ca)† calculated from electron probe average compositions of the starting glasses with ion yields determined from Corning glass standards.

Element	Corning Glasses*	Starting glasses Di_2AbAn	Ak_{80}	Ak_{40}
Ca	1.00	1.00	1.00	1.00
Mg	1.05	1.04	.994	.953
Si	480	.484	.415	.385
Al	1.17	1.19	1.20	1.18
Na	.420	.375	---	---
Sr	.343	.348	.349	.374
Y	.418	.401	.392	.363
Zr	.273	.266	.249	.239
La	.213	.220	.230	.231
Sm	.260	.247	.283	.285
Yb	.183	.189	.200	.193

† $\frac{(I_X/C_X)}{(I_{Ca}/C_{Ca})}$ where I is the ion probe count rate, C is the concentration determined by electron microprobe and X is an element other than Ca.
* Ion yields for Sr, Y, Zr determined from X-glass; La from W-glass; Ca, Mg, Si, Al are averages from V-, W- and X-glasses; see text for Na, Sm, Yb.

determined by EMP analyses are listed in Table 2 (see footnotes to Table 2 for synthesis details). EMP data from each glass composition were collected from several automated straight-line traverses, each containing 13–20 analysis points spaced 10–100 μm apart, depending on the size of the glass chip. For most oxides, 2σ standard deviations in each glass composition are slightly greater than typical 2σ uncertainties expected from counting statistics given in Table 1. Nevertheless, because EMP precision depends upon additional factors, all three glass compositions could be homogeneous in both major and minor elements. Moreover, the coefficient of variation (cv = $100 \times 2\sigma/\bar{x}$) is <4% for most oxides, which is sufficient homogeneity for the purposes of this study. A comparatively wide variation in ZrO_2 concentrations (cv = 10%) was obtained, however, in the Di_2AbAn glass (35-1). Also, in each sample, a systematic variation in SiO_2 was observed as a function of time during typical microprobe sessions (2σ = 0.55–0.77, cv = 1.4–2.6%). Because Si counts were initially collected using a PET crystal in order to optimize spectrometer counting times, the range in concentration of SiO_2 is probably an analytical artifact and not due to sample heterogeneity. This conclusion is based on the occurrence of the Si peak position near the end of the range of spectrometer motion for the PET crystal on the Cameca instrument. Consequently, the Si peak position may not be routinely reproduced with as much precision on PET as on the more routinely used TAP crystal, where the spectral position of Si lies nearer the center of the range of spectrometer motion. We do, however, consider the range in ZrO_2 concentration in 35-1 (0.25 wt%) a real chemical heterogeneity resulting from sample preparation. During this process, minor elements were introduced into the starting mix in the form of an acid solution, but drying the resulting mixture at 1000°C may have produced refractory Zr oxides which were slow to dissolve at the superliquidus temperature of 35-1 (1318°C). A much smaller range of ZrO_2 concentrations is observed in samples Ak_{40}-1 and Ak_{80}-1, consistent with the higher superliquidus run temperatures of these compositions (1526 and 1417°C, respectively). A similar interpretation may apply to the Y_2O_3 analyses (cv = 6–8%). The variation in Na_2O in sample 35-1 (cv = 10%) is assumed to be due entirely to mobilization under the electron beam.

The average composition of the glass starting mixes obtained by IMP using ion yields determined from the Corning glass standards are compared graphically with average electron probe analyses in Fig. 1. Very good agreement is observed between the two analytical techniques in the analysis of the Di_2AbAn glass. The average concentration of each oxide determined by ion probe, with the exception of Na_2O, is within 6% of the average composition obtained by electron probe. Even in the determination of Na_2O, which is difficult by either technique, there is only an ~10% difference in average concentration.

Ion probe analyses of the Ak_{80} and Ak_{40} glasses differ significantly, however, from average electron probe analyses (Fig. 1). The differences are, moreover, systematic: Si, Y, and Zr concentrations are underestimated by the ion probe in both the Ak_{80} and Ak_{40} glass composition by 4–19%, while the remaining elements are overestimated by 1–17%. These results imply that, when high accuracy is desired, ion yields determined from Corning glass standards (and used successfully in analysis of the compositionally similar Di_2AbAn glass) are not applicable to the comparatively SiO_2-poor and CaO-rich melilite compositions.

It is a well-known problem in quantitative ion probe analyses that the ionization probability of a particular element may vary with the concentration of another element—this has been termed the "matrix effect." The ion yields of Ca, Mg, and Ni in the analysis of olivine and clino- and orthopyroxene, for example, have been found to be functions of the concentration of Fe (SHIMIZU et al., 1978; REED et al., 1979; STEELE et al., 1981). SHIMIZU (1986) made a systematic study of the secondary ion emission of Si, Ca, Mg, and Al by analyzing a variety of glass compositions from the systems CaO-Al_2O_3-SiO_2 and MgO-Al_2O_3-SiO_2. It was found that for ion energies less than ~80 eV (which includes the analyses in this study), Ca and Al suppress ionization of Si. Thus, applying the Corning glass ion yields to the Ak_{40} composition resulted in an underestimation of SiO_2 because Al_2O_3 and CaO are ~1.5 and 2.5× higher, respectively, in the melilite composition. CaO has an equivalent concentration in the Ak_{80} glass as in the Ak_{40} composition, but Al_2O_3 is less in the Ak_{80} glass than in the Corning glass. Thus, from the study of SHIMIZU (1986), the difference between ion probe and electron probe determinations of SiO_2 in the Ak_{80} glass should not be as great as in the Ak_{40} glass because only the higher concentration of Ca is contributing to Si suppression. Our results are consistent with this prediction, as SiO_2 is underestimated in the Ak_{80} composition by 13% compared to 19% in Ak_{40}.

Compared to electron probe analyses of the melilite glasses (Fig. 1), most oxides were overestimated by ion probe, while SiO_2 was underestimated. Because the ion probe analyses are normalized to 100%, any analytical error in the concentration of SiO_2 will have a large effect on the normalized concentrations of the other oxides. If the electron probe-determined SiO_2 concentrations are substituted for the ion probe values in both the Ak_{40} and Ak_{80} average analyses and the remaining elements normalized to bring the resulting sum to 100%, then the concentrations of all elements except Zr and Y in Ak_{80}-1 and Zr, Y, and Sr in Ak_{40}-1 are within 7% of the average compositions obtained by electron probe. This cal-

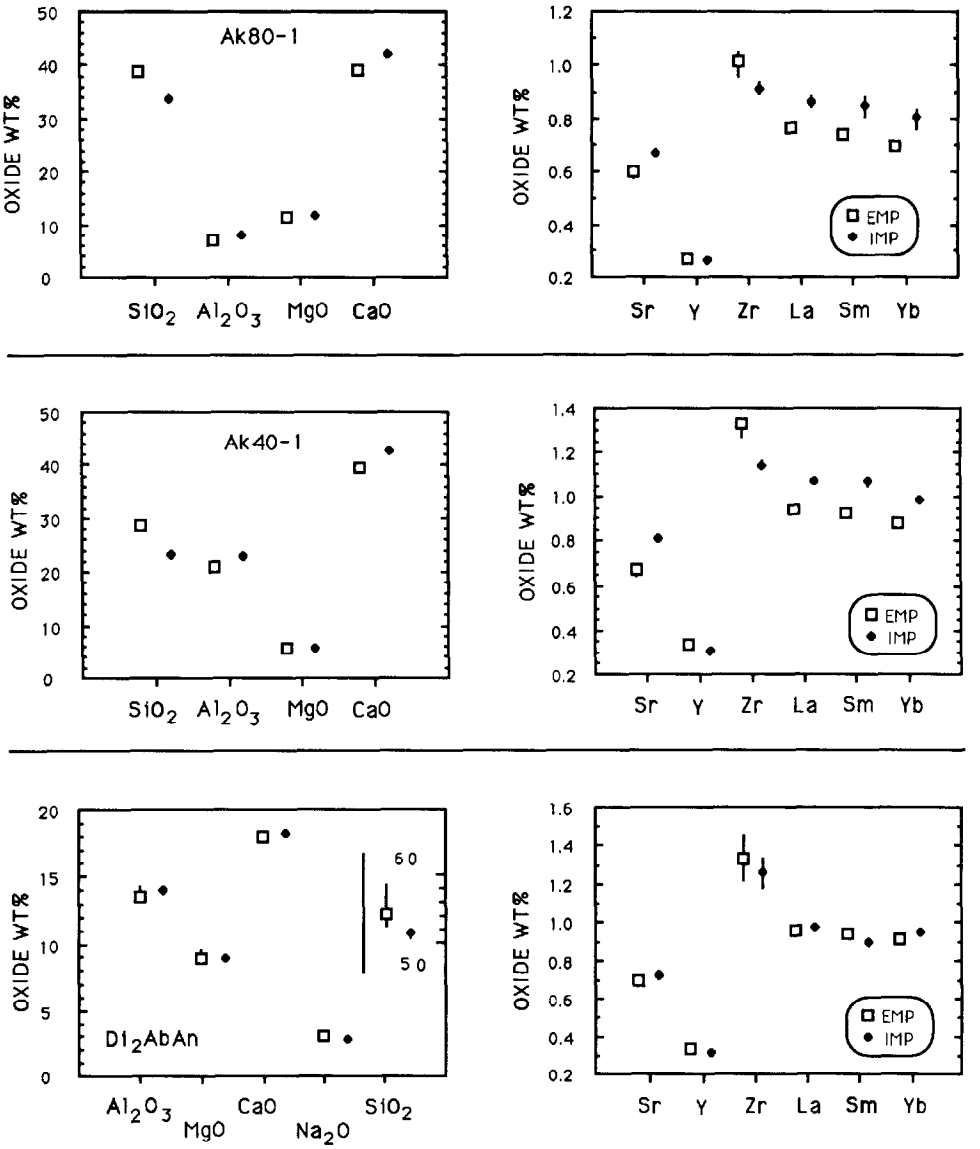

FIG. 1. Comparison of average EMP and IMP determinations of major and trace element concentrations in the synthetic starting glasses. IMP analyses were obtained using ion yields calculated from Corning glass standards. Vertical bars show the range in oxide concentrations for cases where the range is larger than the symbol. Note separate scale for SiO_2 in the Di_2AbAn plot.

culation suggests that variations in the ion yield of Si are the major cause of the erroneous ion probe results for the melilite glass compositions. We do not have an explanation for the irregularities in Sr, Y, and Zr concentrations.

According to the study of SHIMIZU (1986), matrix effects disappear in CMAS compositions when only those ions having energies > 80 eV are analyzed. Although this is a preferred analytical approach, it is not practical for the Chicago instrument because it would result in a significant loss of ion intensity. Because the eventual purpose of our work is in analyzing natural melilite and pyroxene and not in developing analytical techniques for a wide variety of phases, we have corrected for the differences in the analysis of the Di_2AbAn and melilite glasses simply by adopting one set of ion yields for each of the three glasses such that ion probe analyses of each glass composition will reproduce the electron probe-determined averages. A listing of these ion yields is given in Table 3. The new ion yields were used in the analysis of the synthetic crystal/liquid systems. Although the Di_2AbAn glass is compositionally different from crystalline diopside, either set of ion yields on Table 3 (Corning glass or Di_2AbAn) would give the same concentrations for crystalline diopside to within 10%. The melilite glass ion yields will give accurate analyses of crystalline melilite.

Crystal/liquid systems

SEM examination of melilite crystals produced in subliquidus runs from Ak_{80} starting compositions shows that they are $\sim 150 \times 200$ μm in size, they occur singly or in small clusters, and have stout, blocky shapes (Fig. 2). Conical, or sometimes dendritic, overgrowths, ~ 15 μm long, have de-

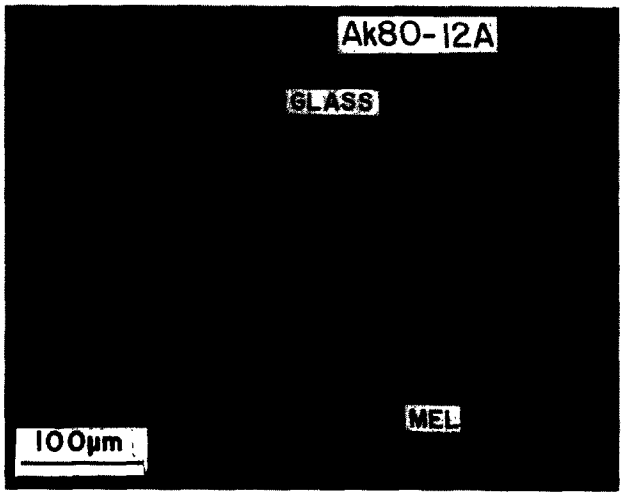

FIG. 2. Backscattered electron image of synthetic melilite grains and glass. Note the bright, trace element-rich boundary layer surrounding each grain and the quench crystal growth on melilite corners. Dark regions at lower right and lower left are epoxy.

veloped on all crystal corners which were in contact with the liquid during quenching. Backscattered electron (BSE) imaging shows that, in addition, a bright fringe region in the glass, ~2 μm wide, borders the outer margin of each melilite grain and grades outward into the adjacent glass. These fringe regions are enriched in the trace elements that are incompatible in melilite (all except Sr), with concentrations up to 3× those in the homogeneous glass away from the crystals. Electron probe traverses across individual melilite grains show that they are Ak_{90} in composition and homogeneous in major elements and SrO. Profiles of minor elements (except Sr), however, show U-shaped composition gradients across the crystals, with progressive enrichment of trace elements toward the rims. Two of these profiles are illustrated in Fig. 3. These profiles cannot be due to contaminating X-rays from the adjacent glass. The homogeneous major element concentrations and possibly the euhedral form of the melilite grains indicate that diffusion of major elements was rapid compared to crystal growth and surface equilibrium was maintained. The fringe regions in the glass, however, represent trace element-rich boundary layers which developed in the liquid adjacent to the growing melilite crystals. Assuming melilite crystal growth occurred over a small fraction of the total run time, it is surprising that such narrow boundary layers were not erased by diffusion. A possible explanation is that precipitation of submicron, incompatible element-rich phases took place in the boundary layer. The fringe regions imply that incompatible element diffusion away from the crystal/liquid interface was slower than crystal growth. This resulted in the regular increase of trace element concentrations in the melilite rim in response to progressive enrichment of minor elements in the adjacent boundary layer during crystallization. As seen in Fig. 2, the boundary layers thin out and disappear around the overgrowths on melilite crystal corners. This indicates that formation of the overgrowths disrupted the boundary layers. Thus, the overgrowths formed last, probably during quenching, and the bright fringes are not quench features.

All melilite grains in the crystal/glass chips examined from Ak_{40} starting compositions are broken crystals. BSE examination of crystal fragments shows that trace element-rich boundary layers also developed in these runs. Random EMP analyses indicate that the melilite grains are Ak_{12} in composition and homogeneous in major element content and in SrO, and that enrichment of minor elements occurs toward crystal margins.

BSE examination of diopside grains produced from Di_2AbAn starting compositions shows that prominent, trace element-rich boundary layers did not form in these charges. EMP analyses of glass adjacent to diopside grains produced in both the isothermal (35-4A) and controlled cooling experiments (35-5B) show that of all trace elements, only ZrO_2 is enriched at the crystal/liquid interface relative to the glass at about 100 μm from the diopside grains, and only by 7%. Even though there was not pronounced boundary layer development in our Di_2AbAn runs, there is a broad range of trace element concentrations in diopside crystals produced in both cooling histories, with individual trace elements varying in concentration by 20–50%. These will be discussed in detail later.

The 35-5B glass is relatively homogeneous, but does show small (5–10%) correlated major element variations lying along a diopside removal trend relative to the starting liquid composition. There are, however, large scale inhomogeneities in the "isothermal" (i.e., rapidly-cooled) sample, 35-4A. In it, the crystals are all localized in one portion of the charge. Regions of glass 300–500 μm from the crystals have a major element composition close to the starting composition but, within about 50–100 μm of the crystals, the glass composition is within the range found for the slowly cooled sample, 35-5B.

Having characterized the crystal/glass samples through detailed EMP and SEM evaluation, IMP analyses were then obtained from these samples using the ion yields calculated from the EMP averages of the starting glass compositions (Table 3). Specifically, the Ak_{80} glass was used as the standard for sample Ak_{80}-12, the Ak_{40} glass for sample Ak_{40}-5A, and the Di_2AbAn glass for samples 35-4A and 35-5B. Because of heterogeneity in the crystalline samples, the average and composition range obtained by EMP and those obtained by IMP are illustrated in Fig. 4 for both glass and crystals in each of the crystal/glass samples. As there are very few cases

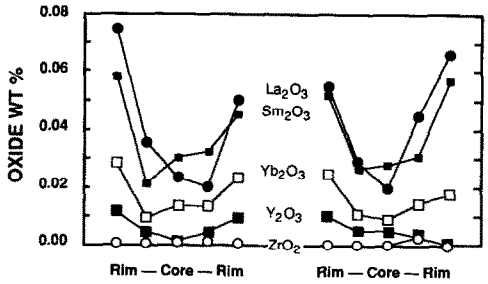

FIG. 3. EMP profiles of minor element oxides across two different synthetic crystals of Ak_{90}. Analysis points are approximately equidistant from one another. Left traverse is 190 μm long. Right is 220 μm long.

in which the identical spot was analyzed by both techniques, the average composition determined by IMP and the average composition determined by EMP are listed for each sample in Table 4.

The comparisons show very good agreement between the averaged IMP and EMP analyses of Ak_{12} and Ak_{90} melilite crystals and their coexisting glasses. For all oxides, the average IMP analysis of the Ak_{12} melilite and coexisting glass agree to within 6% of the EMP average, except for SrO in melilite, which agrees to within 11%. Similarly, the major element oxides in Ak_{90} melilite, and major and trace element oxides in the coexisting glass agree to within 6% of the EMP average. The average trace element oxide concentrations in the Ak_{90} melilite determined by IMP differ from the EMP average by 14% (SrO) to 56% (Yb_2O_3). The dissimilar results for trace element oxides in Ak_{90} melilite, which was analyzed by both techniques concurrently with the coexisting glass, are very likely due only to their low concentrations in this phase, which approach the detection limits of the EMP. The 14% agreement between techniques for SrO is close to the 11% measured in the Ak_{12} melilite, which also has a similar SrO concentration ($\sim$0.6 wt%).

Similar conclusions to those drawn from the comparison of average IMP and EMP melilite compositions result when individual IMP and EMP analyses obtained from the same spot on a melilite grain are examined. Listed on Table 5 are two such comparisons of analyses obtained from spots on Ak_{12} and Ak_{90} melilite crystals. In this table, 2σ, the relative uncertainty in the EMP analysis due only to counting statistics, as well as R, the ratio of the relative difference between IMP and EMP data to 2σ, are given for each oxide. Among major element oxides, when $2\sigma < 2\%$, R can be as large as 3–5. When 2σ is 3–5%, $R < 2$. This indicates that real discrepancies between IMP and EMP data may be present, but only at the several percent level for major element oxides. It is seen that the same holds true for minor element oxides when EMP counting statistics are good, as is the case for the relatively high concentrations found in Ak_{12} melilite. When EMP counting statistics for minor element oxides is poor, as in Ak_{90}, $R < 1$. For both melilite compositions, this indicates excellent agreement between the two techniques for all oxides except SrO, for which the difference between techniques is many times the EMP uncertainty due to counting statistics, although the actual difference is only 15%.

Good agreement is also found between the IMP and EMP average compositions of the glasses coexisting with diopside in the Di_2AbAn experiments (Fig. 4; Table 4). Excluding Na_2O, relative composition differences are <3% in the glass analyses from the controlled cooling sample 35-5B. Relative differences in glass analyses are slightly higher in the isothermal sample (35-4A), but are <12% for all elements. The largest difference (11%) is for MgO, the major element oxide most affected by diopside crystallization. The next largest deviation is for La, which has the lowest D-value among the trace elements studied, thus requiring the largest amount of rehomogenization following diopside crystallization. Even though the diopside from both samples is chemically heterogeneous, good agreement is found between the two analytical techniques when average compositions are compared. For both experimental conditions, agreement is within 16% for all elements and generally within 10%. Given the sample heterogeneities, these are upper limits to any systematic analytical errors. When IMP and EMP analyses of the same spot on a diopside crystal are compared (Table 5), only ZrO_2, Sm_2O_3, and Yb_2O_3 differ by more than can be accounted for by EMP counting statistics, but these differences are <8%.

One of our original reasons for characterizing the three starting glass compositions by EMP was to use them as trace element standards for IMP analyses of crystalline phases in CAIs. One aspect not yet discussed in this regard is the role of structural matrix effects in modifying ion yields. RAY and HART (1982), for example, showed that sputtering of major and trace elements was enhanced by 10–40% in clinopyroxene crystals compared to glasses of similar composition. Consequently, using glass standards could result in erroneous analyses of crystalline phases. In contrast, MUIR and BANCROFT (1987), using a similar instrument but different analytical conditions, found that ion intensities for most major and trace elements varied by less than 10% between glass and crystalline $CaTiSiO_5$. Evaluation of IMP analyses of the melilite and diopside crystals produced in this study with regard to structural matrix effects is somewhat complicated because of the chemical zoning described above. Our results show, however, that if glass standards are used to determine ion yields and if average concentrations in the crystalline phases are considered, SrO is overestimated by the IMP in both melilite compositions compared to the EMP average by 10 and 12%. Thus, enhanced ionization of Sr in crystalline melilite relative to melilite glass may be indicated by our data. Other elements in melilite, and SrO in coexisting glasses (analyzed concurrently with the melilite crystals), show a much closer correspondence between techniques.

In terms of average compositions (Table 4), there is no indication from our data for structural matrix effects in the analysis of diopside-bearing samples using the Di_2AbAn glass standard. A more critical comparison can be made based on an individual IMP analysis and the corresponding point in an EMP line scan of a large, relatively homogeneous (based on EMP data) diopside crystal. Table 5 shows that, except for La, the IMP concentrations are slightly higher, by 5–10%. This is a good comparison, especially since the Di_2AbAn glass used for the ion probe standard differs significantly in composition from the crystalline diopside. Unless there have been fortuitous cancellations, our data suggest that diopside glass is an excellent IMP standard for crystalline diopside. The RAY and HART (1982) results may mean that caution should be used in generalizing this conclusion to all clinopyroxene compositions.

We conclude that by employing ion yields calculated from the average EMP analysis of the starting glass compositions, quantitative determinations of major and trace elements in melilite and diopside can be obtained by IMP techniques that are typically within 10% of those obtained by EMP. As this application of the modified ion yields resulted in quantitative determination of trace elements in synthetic melilite crystals having compositions of Ak_{12} and Ak_{90}, no difficulty is anticipated in using the ion yields for analysis of natural melilite grains in CAIs, which have a similar range in major element composition (Ak_0–Ak_{80}; GROSSMAN, 1980). As the most abundant pyroxene in coarse-grained CAIs is Ti-rich

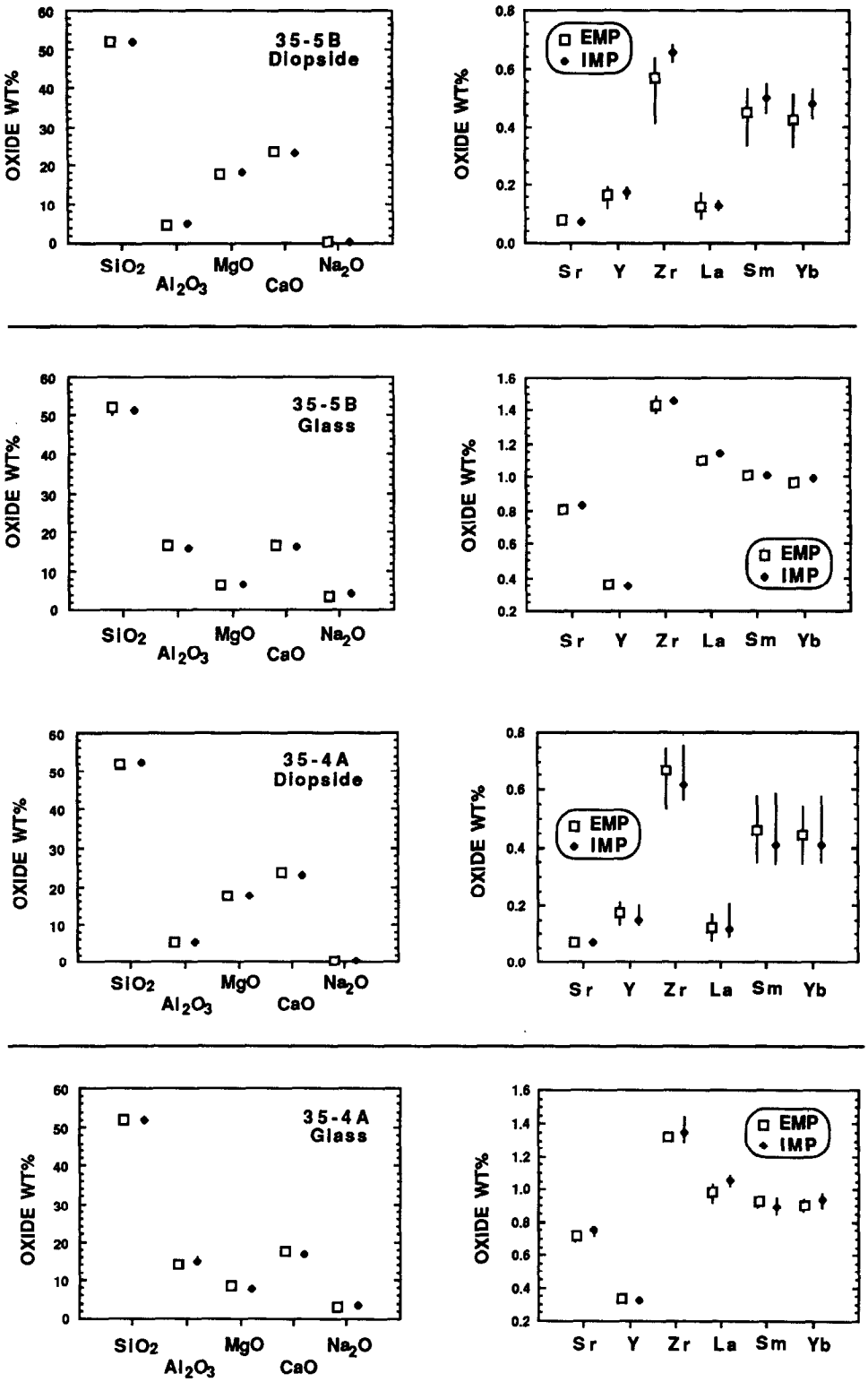

FIG. 4. Comparisons of average EMP and IMP concentrations of major and trace elements in crystals and coexisting glass. Vertical bars show range in oxide concentrations for cases where the range is larger than the symbol. IMP analyses were obtained using ion yields based on the EMP analyses of the synthetic starting glasses. Note scale change for SrO in the Ak_{80}-12A melilite analyses.

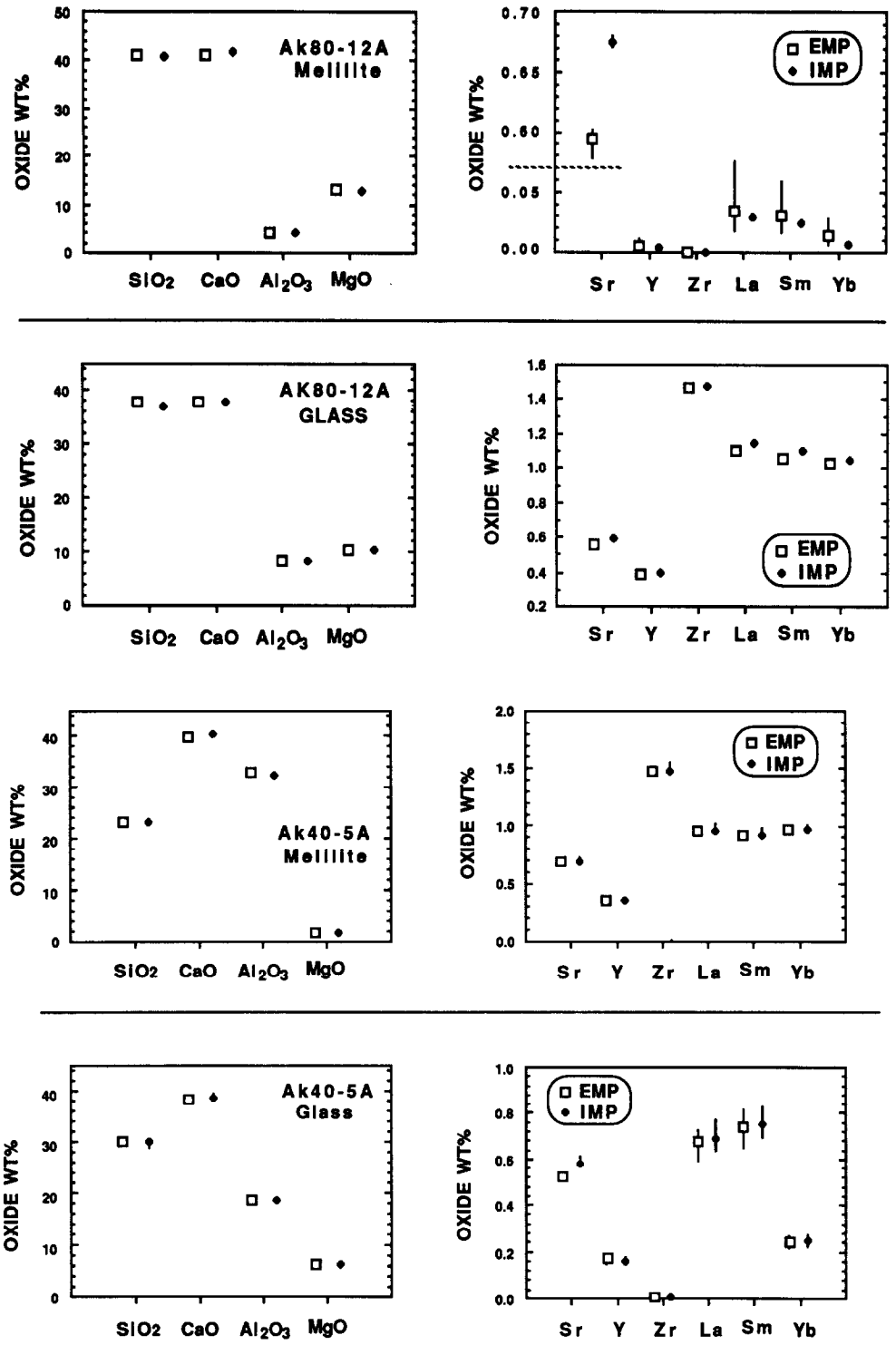

FIG. 4. (Continued)

fassaite, the diopside ion yields obtained here may be of limited usefulness for CAIs.

Melilite/liquid D-values

The purpose of our synthesis experiments was to obtain melilite crystals for IMP/EMP comparisons but, perhaps somewhat surprisingly, reasonable crystal/liquid partition coefficients were also obtained. Because of the U-shaped trace element profiles in the melilite crystals, D-values were calculated using the minor element concentrations obtained from analyses of melilite cores, assuming that the cores crystallized in equilibrium with a liquid which had the compo-

TABLE 4 Comparison of Average+ Electron Probe and Ion Probe Analyses of Crystal/Glass Samples*

SAMPLE	PHASE	SiO_2	Al_2O_3	MgO	CaO	Na_2O	SrO	Y_2O_3	ZrO_2	La_2O_3	Sm_2O_3	Yb_2O_3
	Ak_{90}											
	EMP	41.1	4.26	13.03	41.17	—	594	0046	—	.034	.030	.014
	IMP	40.6	4.04	12.85	41.73	.022	.675	0042	001	.029	024	0062
Ak_{80}-12A	Glass											
	EMP	38.0	8 38	10 21	38.50	—	.556	391	1 467	1 098	1.059	1.027
	IMP	37 1	8.39	10.31	38 45	.013	.593	.395	1.479	1.147	1.105	1.051
	Ak_{12}											
	EMP	23.3	32.83	1 68	39.81	—	.519	.163	—	666	.731	238
	IMP	23.1	32.31	1.65	40 55	.003	.576	.153	.003	.681	743	239
Ak_{40}-5A	Glass											
	EMP	30.2	19.03	6.59	38.99	—	690	.354	1.478	958	.920	963
	IMP	29.0	19.14	6.54	39 68	016	722	.359	1.545	1.015	.975	1 010
	Diopside											
	EMP	51.9	4.70	17.63	23.68	.291	.074	162	.573	121	.448	.425
	IMP	52 1	4 93	17.82	22 80	348	072	.171	.655	.127	.500	.480
35-5B	Glass											
	EMP	51.3	15.96	6 64	16 28	3.37	.807	.357	1 427	1.112	1 008	964
	IMP	51 3	15 79	6.67	16 07	4.37	836	352	1.457	1.145	1.012	993
	Diopside											
	EMP	51.9	5.28	17.53	23.87	.28	.070	171	.665	.123	.461	.442
	IMP	52.5	5.19	17 48	22.76	.28	.069	147	615	.116	407	.406
35-4A	Glass											
	EMP	51 9	13 97	8 53	17.49	2.95	.721	345	1.321	981	934	.906
	IMP	52.1	14.88	7 62	16 75	3 34	.751	.326	1 352	1.056	899	936

* run conditions —
Ak_{80}-12A: 1 hr at 1388°C, 18.5 hr at 1374°C
Ak_{40}-5A: 1 hr at 1495°C, 28 hr at 1474°C.
35-5B: 2 hr at 1270°C, 17 hr at 1260°C, cooled at 2°/hr to 1194°C, held 6 hr.
35-4A: 2 hr at 1270°C, 17 hr at 1260°C, 7-1/4 hr at 1194°C

\+ For EMP, 11-21 spots were averaged for crystals; 19-21 for glasses
For IMP, 5-6 spots were averaged for each sample.

sition of the starting glass. The incompatible element partition coefficients are, strictly speaking, upper limits. In order to minimize errors due to boundary layer effects and recognizing that the plane of a section does not pass through the exact center of each crystal therein, we searched for the melilite grain with the lowest core concentrations of minor elements in each section and used the latter concentrations for determination of *D*-values.

The *D*-values derived from EMP and IMP analyses of melilite are listed in Table 6. As expected from the similarity in trace element concentrations obtained for melilite by the two techniques, IMP *D*-values are very close to EMP *D*-values. *D*-values obtained by the two methods agree to within counting statistics, or 13%, for all elements except Yb, for which they disagree by 45% in Ak_{90}. For clarity, only *D*-values obtained by IMP are plotted in Fig. 5, except for Sr in melilite (plotted in the position of Eu^{2+}), where the EMP value is considered a more reliable determination. The resulting REE *D*-patterns for Ak_{12} and Ak_{90} melilite compositions parallel one another. Each is characterized by nearly constant *D*-values for LREE and progressively decreasing *D*-values for HREE. Our results show that REE^{3+} *D*-values decrease progressively with increasing akermanite content. As the akermanite content of melilite itself increases with decreasing temperature, the effects of melilite composition and temperature are inseparable in our experiments. The REE pattern and absolute *D*-values of our Ak_{12} melilite composition determined by IMP (and EMP) agree very well with

TABLE 5 Single Point EMP-IMP Comparison[a] for Crystalline Melilite and Diopside

Sample	Ak_{80}-12A				Ak_{40}-5A				35-5B			
Method	*IMP*	*EMP*	2σ[b]	$R=\frac{\delta}{2\sigma}$	*IMP*	*EMP*	2σ	$R=\frac{\delta}{2\sigma}$	*IMP*	*EMP*	2σ	$R=\frac{\delta}{2\sigma}$
SiO_2	40.7	41.5	0.4	-5.5	23.0	23.2	0.7	-1.7	52.2	52.3	0.3	-0.5
Al_2O_3	4.15	4.41	3 40	-1.7	32.16	32 91	0.46	-5.0	4 89	4.81	3 12	0.5
MgO	12.81	13 06	0.69	-2 8	1.70	1.66	5.42	0 4	17.85	17.68	0.51	1.9
CaO	41 6	41.4	0.58	1 0	40.6	39.8	0.60	3 1	22 86	23.62	1 02	-3.2
Na_2O									0.334	0.288	6.94	2.3
SrO	0 671	0.602	1.66	6 9	0.605	0.509	1.96	9 6	0.071	0.067	14.93	0.4
Y_2O_3	0.0042	0.006	167	-0.2	0 172	0.171	5 85	0.10	0 153	0.145	6 90	0.8
ZrO_2	0.0008	—	—	—	0.004	—	—	—	0.629	0 575	3.13	3.0
La_2O_3	0 029	0.018	76.9	0.8	0 757	0.719	1.81	2 9	0.113	0.113	11 5	0.0
Sm_2O_3	0.024	0 026	30.8	-0 3	0.821	0.809	0.99	1.5	0 448	0.412	1 94	4.5
Yb_2O_3	0.0059	0.010	40.0	-1.0	0.266	0.260	1.54	1.5	0.430	0.392	1.02	9 5
X_{Ak}	0.903	.886			0 121	0 114						

[a] Analyses refer to same point on same crystal. IMP beam size ~ 10x15 μm, EMP beam size ~ 5 μm.

[b] 2σ is the per cent uncertainty in the EMP analysis due to counting statistics alone.

[c] $\delta=\frac{(C_{IMP}-C_{EMP})}{C_{EMP}} \cdot 100$, where C is the concentration of an oxide.

TABLE 6 Experimental Melilite/Liquid Distribution Coefficients

	Ak_{90}		Ak_{12}	
	EMP	*IMP*	*EMP*	*IMP*
Zr	---	.0023	---	.0010
La	.038	.038	.64	.67
Sm	.035	.032	.72	.75
Sr	.99	1.12	.78	.84
Y	.015	.015	.44	.41
Yb	.019	.0086	.25	.25

INAA results of NAGASAWA et al. (1980), determined from density separates of melilite ($\sim Ak_{15}$) and glass synthesized from a similar starting composition as we have used. Also shown in Fig. 5 are D-values determined by synchrotron radiation XRF analysis by WOOLUM et al. (1988) for Ak_{30} melilite synthesized from an Allende Type B CAI bulk composition. The general shape and intermediate absolute D-values are consistent with D-values determined in this study.

BECKETT et al. (1988) also determined melilite/liquid partition coefficients for several trace elements for a Type B CAI composition, using a technique that allows determination of D-values over a broad range of melilite compositions from only a few experiments. Their results indicate a curvilinear relationship between $D_{La,Ce,Tm}$ and X_{Ak} over the experimental range of $\sim Ak_{25}$–Ak_{70}. Their fitted expression for D_{La} agrees well with our Ak_{90} and Ak_{12} data and with D_{La} for Ak_{15} (0.475) reported by NAGASAWA et al. (1980). Good agreement also exists between D_{Yb} from our data, D_{Yb} for Ak_{30} (0.080) from WOOLUM et al. (1988), D_{Yb} for Ak_{15} (0.222) from NAGASAWA et al. (1980), and D_{Tm} determined from the BECKETT et al. (1988) relationship. The overall agreement shows that melilite composition is more important than bulk composition in determining melilite partitioning behavior in CMAS liquids and also justifies our approach in which D-values were calculated from samples that are strongly zoned in trace elements. Although the general relationships between $D_{REE^{3+}}$ and X_{Ak} defined in the study of BECKETT et al. (1988) may well be correct for melilite of intermediate composition, the relationships cannot hold true for very low X_{Ak} ($\leq Ak_{10}$) as the fitted expressions do not have Y-intercepts. Based on a linear extrapolation of D_{La} from our Ak_{12} data and the Ak_{15} data of NAGASAWA et al. (1980), we estimate D_{La} for Ak_0 $\approx$ 1.35, with La becoming incompatible in melilite ($D_{La} < 1$) at $\sim Ak_6$. The only test of this extrapolation is provided by the measurement of D_{Gd} in Ak_2 by NAGASAWA et al. (1980). Assuming $D_{Gd} \approx D_{La}$, expected from our Ak_{12} data (Fig. 5), this value (1.2) lies directly on the extrapolated line.

In addition to emphasizing the strong effect of melilite composition on partitioning of REE^{3+}, our study of near endmember Ak_{12} and Ak_{90} melilite, analyzed under identical conditions, also reconciles the somewhat conflicting results on the extent of Eu anomalies in melilite found in the data of RINGWOOD (1975), NAGASAWA et al. (1980), and WOOLUM et al. (1988). Both RINGWOOD (1975) and WOOLUM et al. (1988) conclude from the large $D_{Sr}/D_{REE^{3+}}$ ratio of their respective Ak_{70} and Ak_{30} melilite compositions that under reducing conditions melilite should show a large, positive Eu anomaly (assuming $D_{Sr} = D_{Eu^{2+}}$). NAGASAWA et al. (1980) indicate, however, that only a slight positive Eu anomaly should exist, based on analyses of $\sim Ak_{15}$ melilite. In fact, all these results are consistent with one another. As our results show, D_{Sr} varies only slightly over a broad range of X_{Ak} (Fig. 5), whereas $D_{REE^{3+}}$ fall by factors of 18–28 from Ak_{12} to Ak_{90}. As a result, D_{Sr}/D_{Sm} changes from $\sim$1.04 at Ak_{15} to $\sim$31 at Ak_{90}. Thus, it is expected that progressive crystallization of melilite will lead to an increasingly larger positive Eu anomaly when conditions are sufficiently reducing that all Eu is divalent.

Diopside/liquid partitioning

Although the present experiments were carried out for the purpose of IMP-EMP comparisons, the observed incompatible element partitioning in diopside displays some surprising features which, although not completely understood, deserve discussion.

We have systematically examined the EMP data in terms of interelement correlations of "apparent partition coefficients" (C/C_0, where C is the concentration of an element at a given spot on a diopside crystal and C_0 is the initial liquid concentration). The interelement variations of Sm, Y, and Yb display good linear correlations and are consistent with constant partition coefficient ratios: $D(E)/D(Yb)$ = 1.00 and 1.05 for Sm and Y, respectively. All other interelement correlation plots, however, are dominated by scatter (e.g., Figs. 6 and 7). Our diopside synthesis experiments represent about 16% crystallization. If partition coefficients were constant, this amount of fractional crystallization would correspond to at most 16% variation in apparent partition coefficient for the incompatible elements. As illustrated in Figs. 6 and 7, however, all minor and trace elements show much larger variations. These variations show no obvious correlation with crystal location or with clinopyroxene major element composition (e.g., % Tschermak's molecule).

Beyond the predictable effects of fractional crystallization, there are several factors, both equilibrium and kinetic, which can produce both intra- and inter-crystal variations. These include (1) change of partition coefficients with temperature, (2) change in partition coefficients due to the changes in liquid composition that result from progressive crystallization, (3) enhanced incompatible trace element concentrations in the

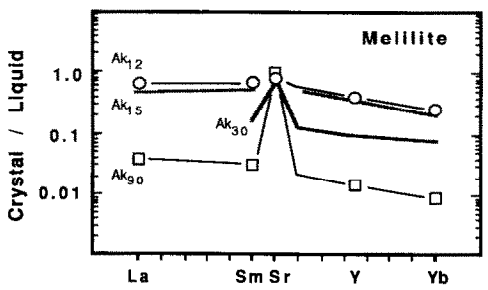

FIG. 5. Melilite/liquid partition coefficients determined in this study, compared to previous studies. Points for Ak_{12} and Ak_{90} from this study; line segments for Ak_{15} from NAGASAWA et al. (1980); line segments for Ak_{30} from WOOLUM et al. (1988).

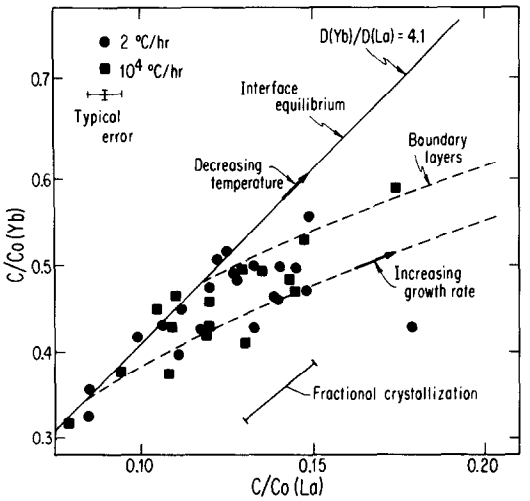

FIG. 6. Correlation plot of apparent diopside/liquid partition coefficients for Yb and La. The error bars represent 2σ uncertainties due to counting statistics for the EMP analysis. The bar labelled fractional crystallization indicates the spread of values expected for this process, assuming constant partition coefficients. The observed variations are much larger. Points from slow- and fast-cooled experiments are indistinguishable. Assuming that the REE partition coefficient pattern does not change with temperature, the line of constant relative partition coefficient, 4.1, can be interpreted as representing crystal regions that grew at interface equilibrium. Points below and to the right of this line could be interpreted as regions whose growth was affected by boundary layers at the crystal-liquid interface. Each dashed line is an illustrative calculation at constant temperature for a region having a varying crystal growth rate. Because every point on the interface equilibrium line is the origin of a boundary layer curve, a scatter of points can be generated. The resultant classification of equilibrium and non-equilibrium points breaks down, however, when data for other elements are compared, casting doubt on boundary layer formation as the origin of the observed scatter.

liquid boundary layer adjacent to the crystal, and (4) anomalous partitioning onto surface sites which do not re-equilibrate once complete coordination is achieved. A special case of (4) is sector zoning, where the surface partition coefficient varies systematically in different crystallographic directions. These mechanisms are not mutually exclusive and might show combined effects, e.g., for (2) and (3). Since the equilibrium liquid composition is itself a function of temperature, we shall regard "temperature" effects to include both mechanisms (1) and (2).

Allowing for the variation of partition coefficients with temperature and assuming interface equilibrium, we expect smooth covariations of apparent partition coefficients among different minor and trace elements. In the special case where the percentage changes in partition coefficient with temperature are the same for a group of elements, straight line plots with constant relative partition coefficient are obtained, as we observe for Sm, Y, and Yb. We interpret the absence of smooth trends as indicative of kinetic effects in partitioning, although smooth interelement correlations do not guarantee interface equilibrium. For example, even if boundary layer effects were important in the partitioning of Sm, Y, and Yb, the observed linear correlations probably would have been preserved, provided that both the partition and diffusion coefficients of these elements are very similar.

Kinetic effects would not have been surprising in the rapidly cooled sample, but it was reasonable to expect that interface equilibrium would be maintained in the slowly cooled sample. Previous fractional crystallization studies have been consistent with this expectation (BENJAMIN et al., 1980, 1983; JONES and BURNETT, 1987; BECKETT et al., 1988).

The 100 micron scale variations in major element composition observed in the glasses of this study are typical for the Di_2AbAn system for the same thermal history (deg/hr cooling rates) as used for sample 35-4A (JONES and BURNETT, 1987; JOHNSON and BURNETT, 1987). The chemical variations indicate that some boundary layer formation did occur during diopside crystallization, although trace element-enriched boundary layers within ~ 10 μm of the diopside crystals were not observed. In the absence of strong composition effects on partitioning, it is not obvious that boundary layers have a major effect on trace element partitioning. As proposed by LINDSTROM (1983), formation of such a boundary layer will slow, possibly stop, crystal growth until the boundary layer is at least partially removed by diffusion of major constituents to the growing interface. Crystal growth and trace element partitioning would then occur only when the boundary layer disappears. Large scale (>100 micron) gradients in glass composition could persist but, as we have observed, there would be no obvious trace element-enriched boundary layers in glass adjacent to crystals.

We now show that it is difficult to explain the observed variability (Figs. 6 and 7) by the presence of boundary layers. If all REE behaved coherently in our experiments, then constant relative partition coefficients would be observed. As discussed above, this is true for Sm, Y, and Yb, but not true (cf. Fig. 6) for La relative to any of the heavier REE; i.e., differences in the diopside REE pattern occur within a single experiment. This incoherence also shows that slow cooling does not guarantee interface equilibrium. Conversely, not all slow cooling experiments show interface disequilibrium. For the same type of cooling history, for example, a linear D_{Pu}-

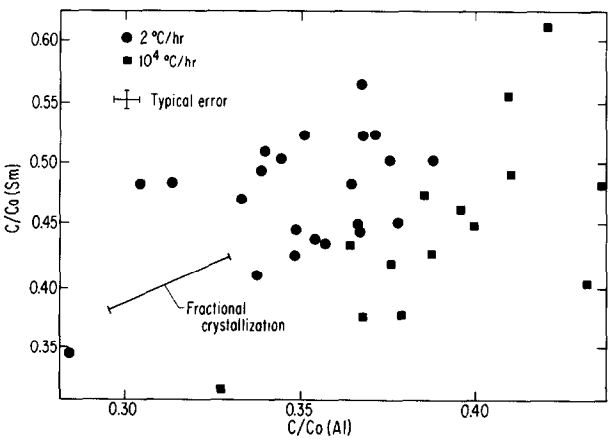

FIG. 7. Correlation plot of apparent diopside/liquid partition coefficients for Sm and Al, analogous to FIG. 6, except that, here, Al partition coefficients are systematically higher for the rapidly cooled sample. A boundary layer interpretation of this plot that would be consistent with FIG. 6 is not possible, suggesting that the scatter in all such correlation plots represents complex surface partitioning processes.

D_{Sm} correlation was obtained by JONES and BURNETT (1987), while the same data (JONES, 1981) show a respectable D_{Al}-D_{Sm} correlation, unlike that found here (Fig. 7).

One possible interpretation of the La data is that, because the partition coefficient of La is significantly lower than any heavy REE, it is much more susceptible to boundary layer formation. Based on the theory of BURTON et al. (1953; cf. JONES and BURNETT, 1987), the apparent partition coefficient depends on the true partition coefficient (for interface equilibrium) and a dimensionless parameter, DEL = vd/D^*, where v is the crystal growth rate, d is the boundary layer thickness, and D^* is the diffusion coefficient. The BURTON et al. (1953) equations are not strictly applicable to these experiments because they assume an infinite reservoir and a steady state but should be adequate to illustrate qualitative systematics. Values for DELs and true partition coefficients define a single point on a correlation plot such as Fig. 6. With variations in crystal growth rate for constant true partition and diffusion coefficients, curved trends of the type illustrated on Fig. 6 result. Recognizing, more realistically, that partition and diffusion coefficients, as well as crystal growth rates, vary with temperature, we can explain a scatter of points, such as that observed in Fig. 6. Predictions of systematics can be made, however, which can be tested with other interelement correlations. Thus, a plausible interpretation of Fig. 6 is that those points which lie on the 4.1:1 correlation line correspond to materials grown at interface equilibrium but at different temperatures. According to this interpretation, those points lying below and to the right of this line have been affected by boundary layer formation.

For a correlation plot using any other pair of elements, an analogous boundary layer interpretation can be developed. The difficulty is that a consistent set of points representing interface equilibrium and points affected by boundary layers cannot be obtained for all elements, even taking liberties with assumed absolute and relative diffusion coefficients. The value of having high precision multielement partitioning data is clear. As a specific example, many of the points defining the 4.1:1 line on Fig. 6 lie in the middle of the clustering of points on Fig. 7. Thus, lack of systematics in the overall data set casts doubt on boundary layers as a general interpretation of the partitioning data presented herein.

We now consider the possibility that our data are dominated by surface partitioning effects (mechanism (4) above). One possible clue is the comparison of the results of the slow (35-5B) and rapidly cooled (35-4A) experiment. Figure 7 shows that the apparent partition coefficients for Al are systematically higher for 35-4A than 35-5B, but those for Sm, La, and Yb are approximately the same in the two experiments (e.g., Fig. 6). Zr is the only other element measured whose apparent partition coefficients are systematically higher in 35-4A than in 35-5B. Of the elements studied, Zr and Al have the highest values of z/r^2 (z = ionic charge, r = ionic radius), the parameter proposed by DOWTY (1976) and SHIMIZU (1981) to govern the chemical differences in sector zoning. It is necessary to assume that systematically different and, presumably, faster-growing sectors grew in the rapidly cooled sample but that the *range* of local partition coefficients was the same for all minor and trace elements other than Al and Zr. Simple sector zoning models, however, in which a different set of constant relative partition coefficients is used for each of two sectors (SHIMIZU, 1981), can be ruled out on the basis of our data. Even if the anomalously high La point on Fig. 6 is arbitrarily excluded, at least three separate constant D(Yb)/D(La) lines would be required to account for the observed variations. If surface partitioning is regarded, however, as a complex interplay between adsorption and desorption, varying with local crystal-melt boundary conditions, then almost any scatter of points might result (SHIMIZU, 1983). We have no better model at present. It is obvious, however, that more appropriate experiments can be done to test these interpretations.

Other workers have observed similar effects in experimental diopside partitioning studies. In a detailed study of the Al_2O_3 content of clinopyroxene in the DiAn system for a wide variety of thermal histories TSUCHIYAMA (1985) demonstrated large increases in Al partition coefficient with cooling rate, qualitatively similar to what we observed. All of his results are interpreted in terms of general "kinetic effects" on partitioning, rather than in terms of any specific mechanism. Detailed EMP contouring of a large crystal showed no obvious Al sector zoning. In contrast, clear sector zoning effects on Al partitioning in diopsidic clinopyroxene grown in the system $CaMgSi_2O_6$-$CaTiAl_2O_6$ were observed by KOUCHI et al. (1983).

Alternatively, the general scatter in trace element correlations that is unique to our work may be due to the high concentrations of "trace" elements employed (about 4% by weight in starting materials). Conceivably, small grains of complex oxides of variable composition might precipitate in association with boundary layer formation and be incorporated as inclusions with subsequent crystal growth. These samples, however, have been well characterized by SEM examination and 1 micron grains of such high atomic number should have been seen. Consequently, we prefer the sector zoning interpretation, although additional experiments would be required to rule out the oxide precipitation hypothesis entirely.

If the qualitative considerations above are correct, we should be able to select those analyses from these complex samples that should best represent equilibrium partitioning and that should be comparable with other diopside partition coefficient measurements in the literature. We now show that this is possible, but the major point is the existence of the kinetic effects, as discussed above.

Because the kinetic effects enhance apparent partition coefficients, the lowest measured concentrations should come from the slow-cooled sample and should yield the best estimates of the partition coefficients at the higher temperature end (1250–1265°C) of the slow cooling stage. An analysis from the central region of a large euhedral crystal ("point 11") gives the lowest concentrations of all elements, except for Sr, whose concentration at point 11 is among the higher measured values. In general, the trend of Sr concentration variations seems to be opposite those of all other incompatible elements. The Sr partition coefficient may be temperature independent or actually decrease with decreasing temperature, consistent with the data of RAY et al. (1983). Partition coefficients based on point 11 and the initial glass composition (D_{min}) are shown on Fig. 8 and listed on Table 7.

An alternative approach is to use rim/glass concentration ratios from the slow-cooled sample to represent partition coefficients appropriate to the low temperature end of the cooling cycle (around 1200°C). The diopside analysis obtained closest to any crystal edge (point 10, 10–15 μm from the crystal-glass interface) defines the partition coefficients labelled "rim" on Fig. 8 and Table 7. The rim partition coefficients are higher than D_{min} for most elements (Zr—65%, REE—50%, Al—10%), but slightly lower than D_{min} for Sr. The principal cause of the rim-D_{min} differences is probably the change in D with temperature, although kinetic effects could also be present.

Our bulk composition is intermediate in the DiAbAn ternary system to the A and B compositions of GRUTZECK et al. (1974), and, except for Sm, our D_{min} for each REE is intermediate between the partition coefficients for the A and B compositions obtained by those authors at a similar temperature. Our D_{min}(Sm) is in reasonable accord with comparable D from RAY et al. (1983) and JONES and BURNETT (1987) (as shown in Fig. 8, inset). D_{min}(Zr) is within 4 and 20% of those of the similar compositions (C2 and C3, respectively) of DUNN and MCCALLUM (1982) which were synthesized at similar temperatures to ours.

Our D_{min}(Al) is 70% higher than that of JONES and BURNETT (1987). This may indicate that there are residual kinetic effects on D_{min} in our experiments and that these are more important for Al than for REE. Alternatively, the difference in D_{min}(Al) between the two studies may reflect a Henry's law deviation in the sense discussed by BENJAMIN et al. (1983). When nominal trace elements, e.g. REE, are at per cent concentrations, as in the present experiments, the necessity of charge balance associated with coupled substitution of the REE $MgAlSiO_6$ component requires that, in general, the partition coefficients for *both* Al and REE cannot be the same as when the REE are at ppm levels, as was the case in the JONES and BURNETT (1987) experiments. It appears, in our experiments, that D_{min}(Al) has increased, with D_{min}(Sm) remaining constant relative to the JONES and BURNETT (1987) work.

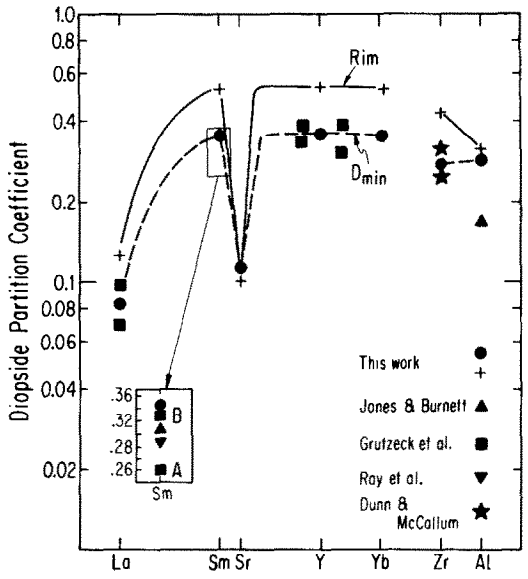

FIG. 8. Diopside partition coefficient patterns for the REE, Zr, and Al. The curve labelled D_{min} is our best estimate of the equilibrium partition coefficient pattern at 1250–1265°C. The curve labelled "rim" is based on crystal rim/glass concentration ratios and is our estimate of partition coefficients at around 1200°C. Except for comparison with D_{Al} from JONES and BURNETT (1987), there is reasonable agreement between our partition coefficients and literature values for comparable bulk compositions and temperatures. Two different compositions from GRUTZECK et al. (1974) are shown. Our composition is intermediate. The reported D_{Sm} of RAY et al. (1983) has been corrected by a factor of 1.4 for IMP matrix effects, as recommended by those authors. D_{Zr} of DUNN and MCCALLUM (1982) is from their compositions C2 and C3.

TABLE 7 Diopside/Liquid Partition Coefficients Estimated in this Work

	D_{min}	D_{rim}
Temperature (°C)	*1250-1265*	*1200*
Al	.28	.31
Sr	.11	.10
Y	.36	.53
Zr	.27	.44
La	.084	.13
Sm	.34	.53
Yb	.34	.53

* Based on analysis of the point with lowest concentrations in the central region of a euhedral crystal and the initial liquid composition.

** Based on analysis of the point closest to the edge of a crystal and the coexisting glass.

SUMMARY AND OVERVIEW

The focus of this study has been to evaluate use of the Chicago ion probe in obtaining quantitative analyses of minor elements in the major phases that are present in natural CAIs. By examining three trace element-doped glasses whose compositions were determined by EMP analyses, we have found that it is not possible to obtain precise quantitative analyses by IMP if there are large differences in SiO_2 content between the standards used to derive the ion yields and the unknowns. Thus, ion yields determined from the three starting glass compositions were used for analysis of synthetic diopside and melilite/glass systems from which crystal/liquid D-values were obtained for trace elements. With the exception of the trace elements in Ak_{90} melilite and SrO in Ak_{12} melilite, resulting IMP analyses using the new ion yields agree with EMP analyses of melilite and coexisting glasses to within 6%. The wider disagreement for trace elements in Ak_{90} melilite is probably due to poor accuracy and precision in the EMP analyses at the low trace element concentrations in this phase. SrO was overestimated by IMP, compared to EMP, in both Ak_{12} and Ak_{90} compositions. This may be the result of a structural matrix effect, as IMP analyses of glass coexisting with diopside agreed to within 3% of the EMP analyses. The somewhat larger deviation between techniques (2 to 16%) found for the diopside analyses may be due to chemical inhomogeneity of the synthetic pyroxene. Thus, IMP techniques used here can be used to acquire quantitative major and trace element analyses of melilite and diopside in natural CAIs.

Taking an extreme point of view, it can be argued that, because the samples discussed herein were not produced at equilibrium, the partitioning results should simply be discarded. There are two questions that have to be answered to evaluate this point of view. First, allowing for the fact that most rocks are not isothermally equilibrated systems, are the experimental conditions and compositions relevant to natural samples? Second, is there anything new in our results? Addressing the second point first, we regard the degree of incoherence between the lithophile trace elements in a slow-cooled sample such as 35-5B as a surprising and interesting result. The fact that we are able to select individual diopside analyses that yield partition coefficients in accord with previous literature values, as shown on Fig. 8, is of lesser importance than the scatter of points on Figs. 6 and 7. It would not have been a particularly interesting result if we had observed linear correlations with the same relative partition coefficients as previously reported in the literature for diopside. The interesting point about the melilite results (Fig. 5) is again not the partition coefficients per se, but that, using common sense in data selection, even from relatively pathological samples, quite reasonable partition coefficients can be obtained relative to those reported in the literature for more-appropriately synthesized samples. It should be emphasized that, in the absence of the literature data, we would have been hesitant to report partition coefficients from these melilite data.

With respect to the first point, we believe that the incompatible element incoherence shown by our diopside quite possibly indicates that significant kinetic effects on trace element partitioning in clinopyroxene can occur at cooling rates that are not excessively high compared to those for some natural samples. For example, our data indicate that the clinopyroxene REE partition coefficient pattern, as measured by Yb/La, could vary by at least 30% due to kinetic effects. Some qualification of this conclusion is required due to the high levels of incompatible lithophile elements in these experiments.

More generally, with the increasing availability of *in situ* trace element microanalytical data, e.g., from ion probes, there is an increasing need to worry about processes leading to inter- and intracrystal variations of trace element contents.

Acknowledgments—We are grateful to I. M. Steele and A. M. Davis for guidance in the operation of the electron and ion microprobes, respectively, and also for their discussions of our results. We thank John Beckett for the melilite starting materials and for helpful discussions, and Astrid Howard for help with synthesis experiments. We profited from discussions with E. Stolper and from reviews by R. Hervig, N. Shimizu, and D. Lindstrom. This work was supported by funds from the National Aeronautics and Space Administration through grants NAG 9-54 (to L. Grossman), NAG 9-94 (to D. S. Burnett), and NAG 9-51 (to R. N. Clayton).

Editorial handling: F. A. Frey

REFERENCES

BECKETT J. R., SPIVACK A. J., HUTCHEON I. D., WASSERBURG G. J., and STOLPER E. M. (1988) The partitioning of trace elements between melilite and liquid: An experimental study with applications to type B CAIs (abstr.). In *Lunar Planet. Sci. XIX*, 49–50. Lunar and Planetary Institute.

BENJAMIN T. M., HEUSER W. R., BURNETT D. S., and SEITZ M. G. (1980) Actinide crystal-liquid partitioning for clinopyroxene and $Ca_3(PO_4)_2$. *Geochim. Cosmochim. Acta* **44**, 1251–1264.

BENJAMIN T. M., JONES J. H., HEUSER W. R., and BURNETT D. S. (1983) Laboratory actinide partitioning: Whitlockite/liquid and influence of actinide concentration levels. *Geochim. Cosmochim. Acta* **47**, 1695–1705.

BURTON J. A., PRIM R. C., and SLICHTER W. P. (1953) The distribution of solutes in crystals grown from the melt. Part I. *Theor. J. Chem. Phys.* **21**, 1987–1991.

DOWTY E. (1976) Crystal structure and crystal growth: II. Sector zoning in minerals. *Amer. Mineral.* **61**, 460–469.

DRAKE M. J. and WEILL D. F. (1972) New rare earth element standards for electron microprobe analyses. *Chem. Geology* **10**, 179–181.

DUNN T. and MCCALLUM I. S. (1982) The partitioning of Zr and Nb between diopside and melts in the system diopside-albite-anorthite. *Geochim. Cosmochim. Acta* **46**, 623–629.

GROSSMAN L. (1980) Refractory inclusions in the Allende meteorite. *Ann. Rev. Earth Planet. Sci.* **8**, 559–608.

GRUTZECK M., KRIDELBAUGH S., and WEILL D. (1974) The distribution of Sr and REE between diopside and silicate liquid. *Geophys. Res. Lett.* **1**, 273–276.

HINTON R. W., DAVIS A. M., SCATENA-WACHEL D. E., GROSSMAN L., and DRAUS R. J. (1988) A chemical and isotopic study of hibonite-rich refractory inclusions in primitive meteorites. *Geochim. Cosmochim. Acta* **52**, 2573–2589.

JOHNSON M. L. and BURNETT D. S. (1987) Henry's Law is obeyed for Tm partitioning into diopside at low concentration (abstr.). *Eos* **68**, 1543.

JONES J. H. (1981) Studies of the geochemical similarity of plutonium and samarium and their implications for the abundance of ^{244}Pu in the early solar system. Ph.D. thesis, Calif. Inst. Tech.

JONES J. H. and BURNETT D. S. (1987) Experimental geochemistry of Pu and Sm and the thermodynamics of trace element partitioning. *Geochim. Cosmochim. Acta* **51**, 769–782.

KOUCHI A., SUGAWARA Y., KASHIMA K., and SUNAGAWA I. (1983) Laboratory growth of sector-zoned clinopyroxenes in the system $CaMgSi_2O_6$-$CaTiAl_2O_6$. *Contrib. Mineral. Petrol.* **83**, 177–184.

KUEHNER S. M., LAUGHLIN J. R., GROSSMAN L., JOHNSON M. L., and BURNETT D. S. (1988) Electron probe and ion probe determination of melilite/liquid and clinopyroxene/liquid partition coefficients of trace elements in CMAS and NaCMAS (abstr.). In *Lunar Planet. Sci. XIX*, 653–654. Lunar and Planetary Institute.

LANGMUIR C. H., BENDER J. F., BENCE A. E., HANSON G. N., and TAYLOR S. R. (1977) Petrogenesis of basalts from the FAMOUS area, Mid-Atlantic Ridge. *Earth Planet. Sci. Lett.* **36**, 133–156.

LINDSTROM D. J. (1983) Kinetic effects on trace element partitioning. *Geochim. Cosmochim. Acta* **47**, 617–622.

MUIR I. M. and BANCROFT G. M. (1987) A comparison of conventional and specimen isolation filtering techniques for the SIMS analyses of geologic materials. *Intl. J. Mass Spectr. Ion Proc.* **75**, 159–170.

NAGASAWA H., SCHREIBER H. D., and MORRIS R. V. (1980) Experimental mineral/liquid partition coefficients of the rare earth elements (REE), Sc and Sr for perovskite, spinel and melilite. *Earth Planet. Sci. Lett.* **46**, 431–437.

PANKHURST R. J. (1977) Open system crystal fractionation and incompatible element variation in basalts. *Nature* **268**, 36–38.

RAY G. and HART S. R. (1982) Quantitative analyses of silicates by ion microprobe. *Intl. J. Mass Spectr. Ion Proc.* **44**, 231–255.

RAY G. L., SHIMIZU N., and HART S. R. (1983) An ion microprobe study of the partitioning of trace elements between clinopyroxene and liquid in the system diopside-albite-anorthite. *Geochim. Cosmochim. Acta* **47**, 2131–2140.

REED S. J. B. (1973) Principles of X-ray generation and quantitative analysis with the electron microprobe. In *Microprobe Analysis* (ed. C. A. ANDERSON), pp. 53–81. Wiley.

REED S. J. B., SCOTT E. R. D., and LONG J. V. P. (1979) Ion microprobe analysis of olivine in pallasite meteorites for nickel. *Earth Planet. Sci. Lett.* **43**, 5–12.

RINGWOOD A. E. (1975) Some aspects of the minor element chemistry of lunar mare basalts. *The Moon* **12**, 127–157.

SHERATON J. W., ELLIS D. J., and KUEHNER S. M. (1984) Rare-earth element geochemistry of Archaean orthogneisses and evolution of the East Antarctic Shield. *BMR J. Australian Geol. Geophys.* **9,** 207–218.

SHIMIZU N. (1981) Trace element incorporation into growing augite phenocryst. *Nature* **289,** 575–577.

SHIMIZU N. (1983) Interface kinetics and trace element distribution between phenocrysts and magma. In *The Significance of Trace Elements in Solving Petrogenetic Problems and Controversies* (ed. S. S. AUGUSTITHIS), pp. 175–195. Theophrastus Publications.

SHIMIZU N. (1986) Silicon-induced enhancement in secondary ion emission from silicates. *Intl. J. Mass Spectr. Ion Proc.* **69,** 325–338.

SHIMIZU N., SEMET M. P., and ALLÈGRE C. J. (1978) Geochemical applications of quantitative ion-probe analyses. *Geochim. Cosmochim. Acta* **42,** 1321–1334.

SMITH J. V. and RIBBE P. H. (1966) X-ray-emission microanalysis of rock-forming minerals III. Alkali feldspars. *J. Geology* **74,** 197–216.

STEELE I. M., HERVIG R. L., HUTCHEON I. D., and SMITH J. V. (1981) Ion microprobe techniques and analyses of olivine and low-Ca pyroxene. *Amer. Mineral.* **66,** 526–546.

STOLPER E. M. (1982) Crystallization sequences of Ca-Al-rich inclusions from Allende: An experimental study. *Geochim. Cosmochim. Acta* **46,** 2159–2180.

STOLPER E. M. and PAQUE J. M. (1986) Crystallization sequences of Ca-Al-rich inclusions from Allende: The effects of cooling rate and maximum temperature. *Geochim. Cosmochim. Acta* **50,** 1785–1806.

TSUCHIYAMA A. (1985) Crystallization kinetics in the system $CaMgSi_2O_6$-$CaAl_2Si_2O_8$: development of zoning and kinetic effects on element partitioning. *Amer. Mineral.* **70,** 474–486.

WOOLUM D. S., JOHNSON M. L., and BURNETT D. S. (1988) Refractory lithophile partitioning in type B CAI minerals (abst). In *Lunar Planet. Sci. XIX,* 1294–1295. Lunar and Planetary Institute.

ZINNER E. and CROZAZ G. (1986) A method for the quantitative measurement of rare earth elements in the ion microprobe. *Intl. J. Mass Spectr. Ion Proc.* **69,** 17–38.